Global and Stochastic Analysis
Vol. 13 No. 3 (2026)

DOI: 10.64837/GSA.13.3.7

Received: 16th April 2026 *Revised: 14th June 2026* *Accepted: 21st June 2026*

COMPARATIVE THERMAL PERFORMANCE ASSESSMENT OF HAMILITON-CROSSER AND XUE MODEL IN POROUS SLIDER VIA L_{16} ORTHOGONAL ARRAY-BASED OPTIMIZATION

G. J. MANJULA, M. KIRANKUMAR, M. J. SRIDEVI*, R. D. JAGADEESHA*, RADHIKA M., C. G. JAGANNATHA, K. C. JAGADEESHA, AND REKHA J.

Abstract. Enhancement of heat transfer efficiency of porous slider systems is of great importance for a wide range of advanced thermal management systems, such as microelectromechanical systems, lubrication technologies, cooling systems, and precision engineering systems. The heat transfer characteristics of nanofluid flow in a porous slider under the combined impact of thermal radiation, heat source/sink and magnetic field is analyzed in the present study. The effect of thermal conductivity is analyzed accurately by comparatively evaluating the Hamilton-Crosser and the Xue thermal conductivity model. Using the appropriate similarity variables the partial differential equations (PDEs) governing the flow and heat transfer processes are transformed to a set of nonlinear ordinary differential equations (ODEs). The subsequent ODEs are solved using the Runge-Kutta-Fehlberg (RKF-45) method to obtain the numerical solutions. Furthermore, Taguchi optimization technique is used to identify the critical parameters affecting the heat transfer rate (H-TR) and to find the optimum operating conditions. The results of the statistical analysis, with coefficient of determination 97.80%, further support the enhanced forecasting ability of the developed optimization model. The maximum H-TR of 1.41595 is obtained at $Rd = 2$, $Q = 0.8$, $Re = 20$, and $\varphi = 0.04$, where the radiation parameter has the most significant impact (50.43%) on the thermal enhancement and the nanoparticle volume fraction has minimal effect (2.27%).

1. Introduction

A key class of engineering surfaces that deliver or remove fluid using a permeable medium are porous sliders. This fluid is injected into the surface and then during motion, the surface creates a lubricating layer that drastically changes the way the fluid moves and its friction. The mechanisms are widely used in hydrostatic bearings, lubrication systems, precision manufacturing equipment and transportation technologies. Its porous structure allows for optimal distribution of pressure and load, ensuring efficient operation and system stability. Further, fluid injection through a porous surface can also postpone the boundary-layer separation and improve thermal management. Because of these benefits, the porous slider configurations are of significant interest in fluid mechanics and tribological studies. They have remained of practical importance, and have encouraged theoretical and computational research into improving flow and heat transfer performance. Alkahtani et al. [2] deliberated the flow of fluid in the presence

2000 *Mathematics Subject Classification.* Primary: 76Dxx, 76S05; Secondary: 80Axx, 65Zxx.
Key words and phrases. Porous slider; Magnetic field; Thermal radiation; Hamilton- Crosser and the Xue thermal conductivity model; Taguchi based optimization.
*Corresponding authors.

of chemical reaction across squeezing porous slider. Turkyilmazoglu [25] addressed the three-dimensional flow inducing porous slider. Faraz et al. [10] scrutinized the effects of magnetic field (M-F) and velocity slip conditions on the viscous fluid flow over a porous slider. Faraz et al. [11] analyzed the behavior of a porous slider subjected to a M-F and slip velocity effects, demonstrating the importance of porous surfaces in fluid flow regulation and drag reduction. The three-dimensional fluid flow of a constant density over a circular porous slider was studied by Madani et al. [15].

The application of M-Fs plays a crucial role in controlling the behavior of electrically conducting fluids, including fluid metals, plasmas, and nanofluids. M-Fs and fluid flow also create magnetohydrodynamic (MHD) forces that can have a significant effect on velocity and temperature distributions. The induced Lorentz force can be used for controlling the flow characteristics, turbulence suppression and thermal performance. The applications of MHD flows include metallurgical processes, cooling systems, power generation, biomedical devices, nuclear engineering and etc. It is very useful to modern technological systems when M-Fs can be used to change the flow of fluid without touching it. Thus, further study of M-F effects continues to be a salient field of study in fluid dynamics. Asjad et al. [4] examined effects of activation energy and M-F on the Williamson fluid flow. Ullah et al. [26] analyzed the effects MHD on electrically conducting fluid flow over a circular porous cylinder. The hybrid nanofluid in a circular porous medium under the influence of a M-F was studied by Izadi et al. [12]. Nabhani and Khlifi [19] investigated the lubrication of non-Newtonian MHD porous squeeze films between circular discs. Reddy et al. [8] studied the flow of MHD fluid in the presence of permeable medium along a stretching cylinder.

Thermal radiation (TR) is one of the basic mechanisms of heat transfer that is more significant at high temperatures. TR is a process of energy transfer that does not need a medium, unlike conduction and convection. Temperature distribution in industrial furnaces, solar collectors, gas turbines, spacecraft, and energy systems is greatly influenced by radiative heat transfer. TR may be either a positive or a negative effect on thermal flow in flow problems. This addition of radiation effects provides for more realistic thermal models in applications that are at high temperature. For that reason, TR still remains an important factor in the field of advanced heat transfer research. Mahmoud [16] investigated the effects of heat radiation and changing thermal conductivity (T-C) on a deformable surface. Bataller [5] investigated the impact of heat radiation on the flow of a viscoelastic fluid over to an expanding surface. Kumar et al. [13] investigated the effects of TR and heat transfer on the mobility of nano-fluid across a vertical plate. Kumar et al. [23] investigated the mixed convective fluid flow in the presence TR. Bharath Kumar et al. [6] studied the reactive fluid flow subjected to two parallel disks with TR effect.

Anwar et al. [3] investigated the flow of nano-fluid across a Darcy medium, considering the effects of a heat source and TR.

Predicting accurately the T-C of nanofluids plays vital role when dealing with heat transfer performance of nanofluids. In the theoretical models that have been widely used, the Hamilton–Crosser and Xue models have been the subject of much interest because they can describe various characteristics of nanoparticles. The Hamilton–Crosser model incorporates the effect of particle shape and is applicable to those nanofluids that contain non-spherical nanoparticles, while the Xue model is a specially developed model for carbon nanotube–based nanofluids, which accounts for the unique structural properties of the carbon nanotube. They give better estimates of the effective T-C than the conventional models, and have been widely used in fluid flow and heat transfer studies. Their application helps to create more realistic thermal transport phenomena in nanofluids which are useful tools for advanced thermal systems and engineering processes. In order to examine dual solutions and T-C in hybrid nanofluids, Sarfraz et al. [22] compared the Xue and Hamilton-Crosser models. Using Hamilton-Crosser and Xue models, Galal et al. [9] investigated the potential of trihybrid nanofluid and TR for enhancing flow and heat transmission in industrial processes. The effect of the Hamilton-Crosser model on particles in a nanofluid flow (NF-F) impacted by varying T-C was investigated by Alharbi et al. [1]. Using particle clustering and nanolayer creation, Wang et al. [27] investigated the reconstruction of the Hamilton-Crosser model for nanofluid effective T-C. A comparison of Xue and Hamilton-Crosser nanofluid models for the best use of solar energy in cylindrical Prandtl ferrofluid film flow was conducted by Sandeep et al. [21].

The Taguchi method is a statistical optimization method that is developed to enhance the performance of a process with minimum number of experimental or computational runs. Uses orthogonal array and signal-to-noise (SN) ratio to identify the optimum parameter combination in an efficient manner. It is a method which is widely used in engineering, manufacturing, fluid mechanics and heat transfer applications to analyze the effect of more than one control factor. It has several benefits including the reduction of computational costs and time for determining significant parameters. Taguchi analysis can also be used to achieve robust design which reduces sensitivity to external disturbance and uncertainties. The Taguchi method is a very simple and efficient optimization method and is widely used in science and engineering research. Raei [20] used the Taguchi approach to examine the statistical analysis of nanofluid heat transfer. Darbari and Alavi [7] conducted a numerical investigation of fluid flow and heat transmission in a flat tube using the Taguchi technique. Kumar et al. [14] conducted an entropy study of thermos-diffusive flow on a curved sheet using the Taguchi technique. Mishra et al. [18] investigated the Taguchi statistical analysis in the context of Marangoni convective NF-F across an infinite porous disk. Majumder et al. [17] investigated the Taguchi analysis of heat transmission in NF-F across a rotating sphere. The chemically reactive and radiative hybrid nanofluids flow due to moving flat plates was studied by Tejaswini et al. [24].

A comprehensive review of the literature reveals that no previous research has investigated the combined effects of M-F, TR, and heat source/sink (HS-S) on NF-F across a porous slider. The distinctiveness of this work arises from the combination of comparative T-C predictions developed using the Hamilton-Crosser model and the Xue model. The examination of NF-F and thermal transfer in porous slider is conducted owing to its increasing significance in contemporary thermal managements systems, where effective heat dissipation and flow regulation are crucial for improved performance. The controlling nonlinear PDEs are converted into coupled ODEs through the use of similarity variables, and the resulting equations are solved with the RKF-45 method. The influence of critical regulating factors on the H-TR of the ferrofluid system is systematically analyzed and optimized using the Taguchi statistical method. The existing framework may serve as an advantageous instrument for the design of magnetic cooling systems, rotating thermo-mechanisms, ferrofluid energy transfer systems, and sophisticated thermo-engineering applications concerning the transport of magnetic nanoparticles.

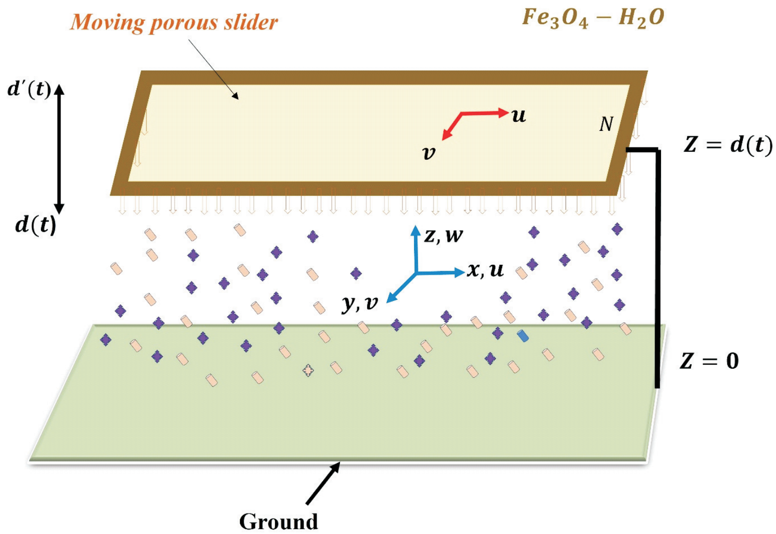

FIGURE 1. Flow geometry.

2. Mathematical formulation

This study examines a three-dimensional unsteady NF-F originated by porous slider that expands and contracts, influenced by M-F, and radiative heat transfer. The slider can traverse the three dimensional (x, y, z) axis, with the z-axis representing the vertical movement direction. The downward motion, defined by the velocity $\dot{d}(t)$ of and the separation distance $d(t)$ between the surfaces is presumed to be significantly lower than the dimensions of the sliders in the x and y directions. In addition, U and V represent the constant sliding velocities of the flat slider along x and y axis, respectively, while the slider is sustained aby a time varying fluid injection originating from its base with velocity $W(t)$ is visualized in Figure 1. The HS-S are analyzed to evaluate heat transmission. The governing equations for the fluid flow, incorporating the pressure and velocity fields, are provided by

$$u_x + u_y + u_z = 0, \tag{1}$$

$$u_t + vu_y + uu_x + wu_z + \frac{1}{\rho_{nf}}p_x = \upsilon_{nf}[u_{xx} + u_{zz} + u_{yy}] - \frac{\sigma_{nf}}{\rho_{nf}}B_0^2 u, \tag{2}$$

$$v_t + uv_x + vv_y + wv_z + \frac{1}{\rho_{nf}}p_y = \upsilon_{nf}[v_{xx} + v_{yy} + v_{zz}] - \frac{\sigma_{nf}}{\rho_{nf}}B_0^2 v, \tag{3}$$

$$ww_z + w_t + vw_y + uw_x + \frac{1}{\rho_{nf}}p_z = \upsilon_{nf}[w_{xx} + w_{yy} + w_{zz}] - \frac{\sigma_{nf}}{\rho_{nf}}B_0^2 w, \tag{4}$$

$$T_t + uT_x + vT_y + wT_z = \frac{k_{nf}}{(\rho C_p)_{nf}}[T_{xx} + T_{yy} + T_{zz}] + \frac{16\delta^* T_0^3}{3k^*(\rho C_p)_{nf}}T_{zz} + \frac{Q_0}{(\rho C_p)_{nf}}(T - T_0). \tag{5}$$

Under suitable boundary conditions,

$$w = 0,\ u = U,\ v = V, T = T_h, \quad \text{at } z = 0,$$
$$w = -W(t),\ u = 0, v = 0,\ T = T_0, \quad \text{at } z = d(t). \tag{6}$$

The similarity variables used in the present study are delineated as follows,

$$u = Uf(\eta) + \frac{W(t)}{d(t)} x h'(\eta),\ v = Vg(\eta),$$
$$w = -W(t)h(\eta), \eta = \frac{z}{d(t)},\ \theta = \frac{T - T_0}{T_h - T_o}. \tag{7}$$

The reduced form of equation (2)–(5) are obtained using equation (7), given as,

$$\frac{\upsilon_{nf}}{\upsilon_f} h'''' + S[2h'' + \eta h'''] + Re[hh''' - h''h'] - \frac{\sigma_{nf}}{\sigma_f}\frac{\rho_f}{\rho_{nf}} Mh'' = 0, \tag{8}$$

$$\frac{\upsilon_{nf}}{\upsilon_f} f'' + S\eta f' + Re\,[hf' - h'f] - \frac{\rho_f}{\rho_{nf}}\frac{\sigma_{nf}}{\sigma_f} Mf = 0, \tag{9}$$

$$\frac{\upsilon_{nf}}{\upsilon_f} g'' + Rehg' + S\eta g' - \frac{\sigma_{nf}}{\sigma_f}\frac{\rho_f}{\rho_{nf}} Mg = 0, \tag{10}$$

$$\frac{(\rho C_p)_f}{(\rho C_p)_{nf}} \frac{1}{\Pr} \left[\frac{k_{nf}}{k_f} + Rd\right] \theta'' + Reh\theta' + S\eta\theta' + \frac{(\rho C_p)_f}{(\rho C_p)_{nf}} Q\theta = 0. \tag{11}$$

The modified boundary settings are represented as follows,

$$h(0) = 0,\ h'(0) = 0, f(0) = 1, g(0) = 1, \theta(0) = 1,$$
$$h'(1) = 0,\ h(1) = 1,\ f(1) = 0, g(1) = 0,\ \theta(1) = 0. \tag{12}$$

The dimensionless variables are as follows,

$$Re = \frac{d(t)W(t)}{\upsilon_f}, M = \frac{\sigma_f}{\rho_f}\frac{B_0^2}{\upsilon_f}(d(t))^2, Rd = \frac{16\delta^* T_0^3}{k^* k_f}, S = \frac{d(t)\dot{d}(t)}{\upsilon_f},$$
$$\Pr = \frac{(\mu C_p)_f}{k_f}, Q = \frac{Q_0 (d(t))^2}{\upsilon_f (\rho C_p)_f}. \tag{13}$$

3. Numerical scheme and convergence criteria

The governing equations for the current model can be expressed as a highly nonlinear and intricately connected system of partial differential equations that delineate the fundamental transport processes. The presence of multiple independent variables renders the derivation of explicit solutions to these equations exceedingly challenging. The implementation of the transformations enables the reformulation of the original differential equations (1)–(5) and their associated boundary conditions (6) into dimensionless ordinary differential equations (8)–(11), along with the modified boundary conditions (12). The resulting equations are strongly nonlinear and coupled which are solved numerically using RKF-45 method to obtain an accurate solution. The thermophysical properties

TABLE 1. Thermophysical properties of NF.

Properties	**Correlation**
Dynamic viscosity model	$\frac{\mu_{nf}}{\mu_f} = \frac{1}{(1-\varphi)^{2.5}},$
Density model	$\frac{\rho_{nf}}{\rho_f} = (1-\varphi) + \varphi\frac{\rho_s}{\rho_f}$
Heat capacity model	$\frac{(\rho C_p)_{nf}}{(\rho C_p)_f} = (1-\varphi) + \varphi\frac{(\rho C_p)_s}{(\rho C_p)_f}$
Electrical conductivity model	$\frac{\sigma_{nf}}{\sigma_f} = 1 + \frac{3(\sigma-1)\varphi}{(\sigma+2)-(\sigma-1)\varphi}$ where $\sigma = \frac{\sigma_s}{\sigma_f}$
Xue T-C model	$\frac{k_{nf}}{k_f} = \frac{1-\varphi+2\varphi\left(\frac{k_s}{k_s-k_f}\right)\ln\left(\frac{k_s+k_f}{2k_f}\right)}{1-\varphi+2\varphi\left(\frac{k_f}{k_s-k_f}\right)\ln\left(\frac{k_s+k_f}{2k_f}\right)}$
Hamilton Crosser T-C model	$k_{nf} = k_f\frac{k_p+(n-1)k_f+(n-1)(k_p-k_f)\varphi}{k_p+(n-1)k_f-(k_p-k_f)\varphi}$

TABLE 2. Base fluid and nanoparticle thermophysical characteristics.

Properties	Fe_3O_4	H_2O
ρ	3600	997.1
k	9.7	0.613
C_p	670	4179
σ	0.74×10^{-6}	0.05

and their corelation is given in Table 1 and Table 2. For numerical computation, the above equations are converted to first order equations as described below.

$$\left.\begin{aligned} &h = \Gamma_1, h' = \Gamma_2, h'' = \Gamma_3, h''' = \Gamma_4 \\ &f = \Gamma_5, f' = \Gamma_6, g = \Gamma_7, g' = \Gamma_8, \\ &\theta = \Gamma_9, \theta' = \Gamma_{10}, \end{aligned}\right\} \tag{14}$$

Substituting equation (14) into the transformed equations,

(15)

$$\Gamma_4' = -\frac{\mu_f}{\mu_{nf}}\frac{\rho_{nf}}{\rho_f}\left(Re(\Gamma_1\Gamma_4 - \Gamma_2\Gamma_3) + S(2\Gamma_3 + \eta\Gamma_4) - \frac{\sigma_{nf}}{\sigma_f}\frac{\rho_f}{\rho_{nf}}M\Gamma_3\right),$$

(16)

$$\Gamma_6' = -\frac{\mu_f}{\mu_{nf}}\frac{\rho_{nf}}{\rho_f}\left(Re(\Gamma_1\Gamma_6 - \Gamma_2\Gamma_5) + S\eta\Gamma_6 - \frac{\sigma_{nf}}{\sigma_f}\frac{\rho_f}{\rho_{nf}}M\Gamma_5\right),$$

(17)

$$\Gamma_8' = -\frac{\mu_f}{\mu_{nf}}\frac{\rho_{nf}}{\rho_f}\left(Re\Gamma_1\Gamma_8 + S\eta\Gamma_8 - \frac{\sigma_{nf}}{\sigma_f}\frac{\rho_f}{\rho_{nf}}M\Gamma_7\right),$$

(18)

$$\Gamma_{10}' = -\frac{1}{\Pr\left(\frac{k_{nf}}{k_f} + Rd\right)\frac{(\rho C_p)_f}{(\rho C_p)_{nf}}}\left(Re\Gamma_1\Gamma_{10} + S\eta\Gamma_{10} + \frac{(\rho C_p)_f}{(\rho C_p)_{nf}}Q\Gamma_9\right).$$

(19)

$$\Gamma_1(0),\ \Gamma_2(0),\ \Gamma_5\,(0) - 1,\ \Gamma_7(0) - 1, \Gamma_9(0) - 1,\ \Gamma_1(1) - 1,\ \Gamma_2(1),\ \Gamma_5(1),\ \Gamma_7(1), \Gamma_9(1).$$

4. Taguchi Method

The Taguchi method has become prominent as an efficient optimization technique in many engineering disciplines. It provides a systematic methodology to obtain optimum performance from the system design. The Taguchi approach with orthogonal arrays was used to develop the optimization model which is subsequently verified analysis of variance (ANOVA). The combination of methodologies made possible the identification of parameters and validation of the optimal solution. This methodology has several advantages such as less computing load, better efficiency and better reliability in the parameter evaluation. The selected control variables for process optimization comprised radiation parameter, HS-S parameter, Reynolds number, and nanoparticle volume fraction are detailed in Table 3.

TABLE 3. Specification of control parameters and corresponding level settings.

Input parameters	**Symbols**	**Setting-1**	**Setting-2**	**Setting-3**	**Setting-4**
Radiation parameter	A	2	4	6	8
HS-S parameter	B	0.2	0.4	0.6	0.8
Reynolds number	C	5	10	15	20
Nanoparticle volume fraction	D	0.01	0.02	0.03	0.04

Four control parameters with 4 levels each were used for the optimization framework. A full factorial approach would need 256 simulation cases to evaluate all combinations of the parameters. Such an exhaustive analysis would be time consuming and would require a lot of computation because of the nonlinear nature of the present problem. In order to overcome this drawback, Taguchi methodology was used. A numerical design space was selected using an L_{16} orthogonal array, which provided a good representation of the design space with significantly fewer numerical trials. The number of simulations required was decreased from 256 to 16, but the quality of the statistical analysis remained the same. The corresponding orthogonal array is shown in Table 4.

The quantity of control factors, the levels assigned for each of the control factors, and the number of degrees of freedom for each of the control factors determine the appropriate orthogonal array for the Taguchi methodology. The current computation involves 4 parameters, each evaluated at 4 different levels. A matrix was required to implement this factor level design according to the Taguchi design criteria. The optimal design

TABLE 4. L_{16} orthogonal array of representing factor level combinations.

Runs	$\boldsymbol{A}$	$\boldsymbol{B}$	$\boldsymbol{C}$	$\boldsymbol{D}$	$\boldsymbol{-\theta'(0)}$	**SN ratio**
1	2	0.2	5	0.01	1.10621	0.87677
2	2	0.4	10	0.02	1.20542	1.62279
3	2	0.6	15	0.03	1.30970	2.34344
4	2	0.8	20	0.04	1.41595	3.02096
5	4	0.2	10	0.03	1.11269	0.92752
6	4	0.4	5	0.04	1.05253	0.44471
7	4	0.6	20	0.01	1.22479	1.76122
8	4	0.8	15	0.02	1.16070	1.29441
9	6	0.2	15	0.04	1.11709	0.96177
10	6	0.4	20	0.03	1.15575	1.25727
11	6	0.6	5	0.02	1.03299	0.28195
12	6	0.8	10	0.01	1.06863	0.57657
13	8	0.2	20	0.02	1.11963	0.98147
14	8	0.4	15	0.01	1.08624	0.71850
15	8	0.6	10	0.04	1.05421	0.45854
16	8	0.8	5	0.03	1.02300	0.19755

identified is the L_{16} orthogonal array, which is effectively accommodates 4 parameters at 4 levels, ensuring high degree of statistical balance and low computational effort.

The SN ratio was used as the measure of the response characteristics. Considering all the objectives of this study, the “larger-the-better” quality characteristic was used to optimize the $-\theta'(0)$. The formula for the calculation of the corresponding SN ratio is presented in Eq. (20).

$$S/N = -10 \log \left(\frac{1}{\beta}\right) \sum \frac{1}{\xi^2}, \tag{20}$$

The SN analysis for heat transfer performance has been conducted and is displayed in Table 5. Table 5 indicates that the parameter combination $A_2, B_{0.8}, C_{20}$, and $D_{0.04}$ yields the highest $-\theta'(0)$ among all configurations. Consequently, this parameter configuration is excellent for heat transfer performance.

TABLE 5. SN ratio for $-\theta'(0)$.

Level	**A**	**B**	**C**	**D**
1	1.9660	0.9369	0.4502	0.9833
2	1.1070	1.0108	0.8964	1.0452
3	0.7694	1.2113	1.3295	1.1814
4	0.5890	1.2724	1.7552	1.2215
Delta	1.3770	0.3355	1.3050	0.2382
Rank	1	3	2	4

ANOVA was used to test the statistical significance of selected governing parameters and to verify the usefulness of the regression model obtained. Table 6 presents the contribution percentages and significance values of individual control factors for the $-\theta'(0)$, matching to the ANOVA results. In order to test the ability of the model being developed to predict accurately, the coefficient of determination R^2 and the adjusted coefficient of determination R^2 were also computed. The values of 97.80% and 88.98% respectively are obtained, which shows a good correlation between the regression and the numerical simulation data. The obtained results verify that the developed model represents the variation in the heat transfer response with a high fidelity, and can be relied upon for prediction in the range of the studied parameters. The statistical analysis results allow for the formulation of the predictive connection for the $-\theta'(0)$ as follows:

$$-\theta'(0) = 1.14035 + 0.1190A_2 - 0.0027A_4 - 0.0467A_6 - 0.0696A_8 - 0.0264B_{0.2} - 0.0154B_{0.4} + 0.0151B_{0.6} + 0.0267B_{0.8} - 0.0867C_5 - 0.0301C_{10} + 0.0281C_{15} + 0.0887C_{20} - 0.0189D_{0.01} - 0.0107D_{0.02} + 0.0099D_{0.03} + 0.0196D_{0.04}. \tag{21}$$

TABLE 6. ANOVA for selected performance measure of $-\theta'(0)$.

Source	D-F	Adj S-S	Adj M-S	F-Value	p-Value	% impact
A	3	0.084747	0.028249	22.87	0.014	50.43
B	3	0.007506	0.002502	2.03	0.288	4.47
C	3	0.068280	0.022760	18.43	0.020	40.63
D	3	0.003812	0.001271	1.03	0.491	2.27
Error	3	0.003705	0.001235			2.20
Total	15	0.168050				

The ANOVA results indicate that parameter A is the most significant factor, accounting for 50.43% of the variation in the response variable, while parameter C follows as the next most influential, contributing 40.63% to the variance of the response variable. The effects of parameters B and D are comparatively minor, at 4.47% and 2.27%, respectively. The error contribution is 2.20%, confirming the sufficiency of the experimental design and indicating that the chosen parameters adequately account for nearly all observed variability in the response. The p-value test indicates that component A ($p = 0.014$) and factor C ($p = 0.020$) significantly influence the response variable, whereas factors B and D have negligible effects regarding their parameters.

5. Results and Discussion

The nanofluid flow produced by the porous slider under the impact of radiative heat transfer, HS-S, and M-F is investigated in the present study. The effect of T-C on the H-TR is evaluated using both Hamilton-Crosser model and the Xue model. Similarity transformation is employed to transform the momentum and energy equations to ODEs for simplified numerical analysis. The transformed equations are solved numerically by the RKF-45 method. In this section, the influence of various dimensionless parameters on velocity and temperature profiles is discussed to analyze the practical applicability of the model.

Figure 2 illustrates the impact of the S on the velocity distribution $h'(\eta)$. As the distance between the two sliders decreases, the confined NF-F faster through the narrowing channel. Nonetheless, this increase does not occur uniformly within the domain. As the sliders expands, fluid flow becomes weaker because of the lesser compression force and

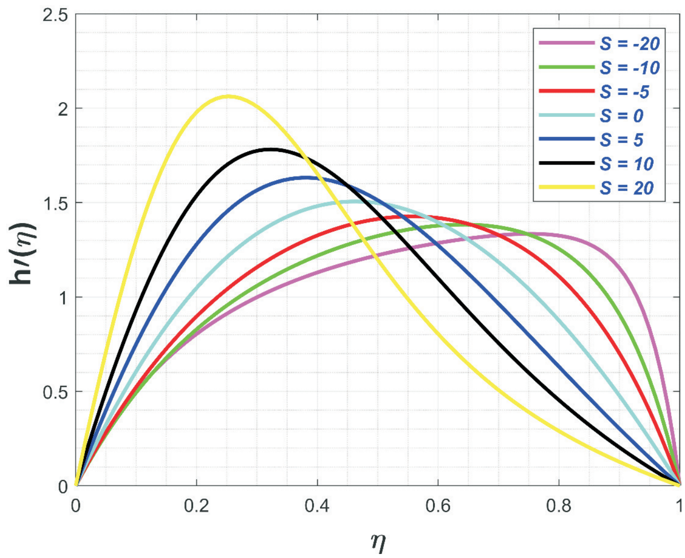

FIGURE 2. The consequence of S on $h'(\eta)$.

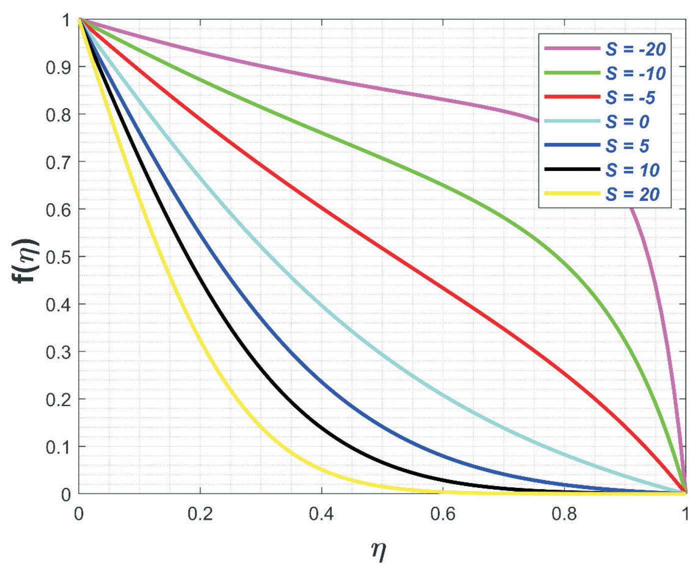

FIGURE 3. The consequence of S on $f(\eta)$.

greater resistance to flow. A considerable secondary flow pattern appears in the central part of the channel. The effect of the S on the $f(\eta)$ and $g(\eta)$ are shown in Figures 3 and 4. The velocity function $g(\eta)$ dominates the velocity function $f(\eta)$.

Figures 5, 6 and 7 shows the effects of M on the $h'(\eta)$, $f(\eta)$ and $g(\eta)$. An increase in the value of M slightly increases the $h'(\eta)$ at both the upper and lower plates, but

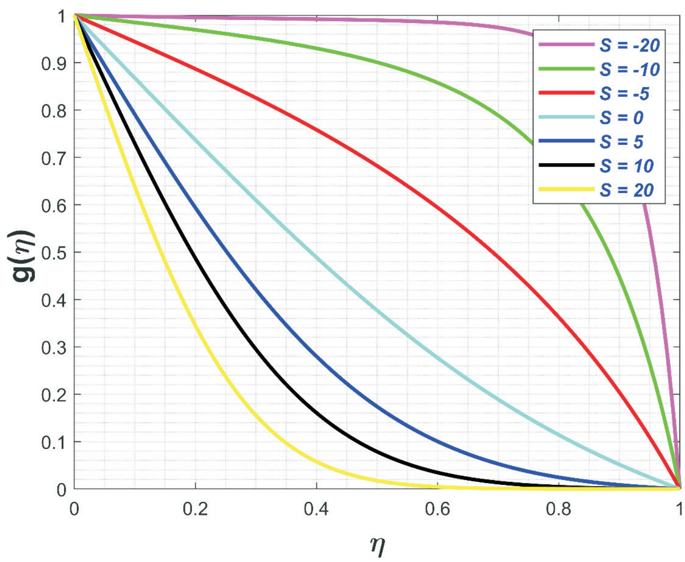

FIGURE 4. The consequence of S on $g(\eta)$.

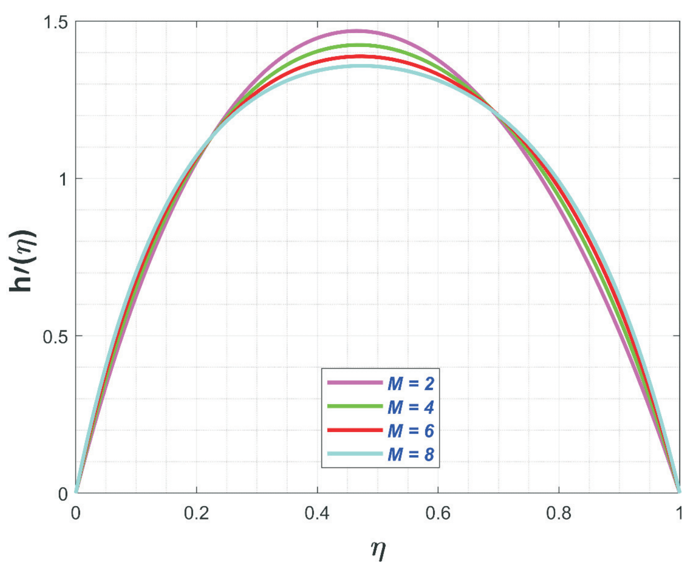

FIGURE 5. The consequence of M on $h'(\eta)$.

a large decrease is noted at the centre region. The fluid in the central region has more longitudinal speed, which implies that the Lorentz force will be more significant compared to the adjacent fluid. The Lorentz force acts as a dissipative force that restricts the fluid flow.

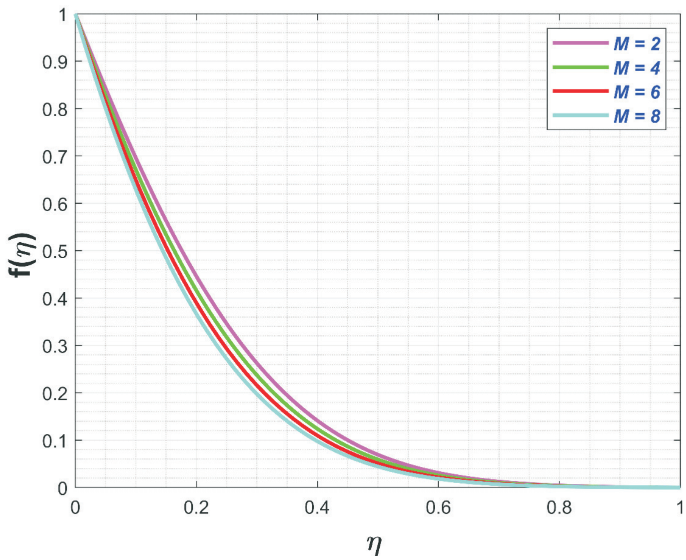

FIGURE 6. The consequence of M on $f(\eta)$.

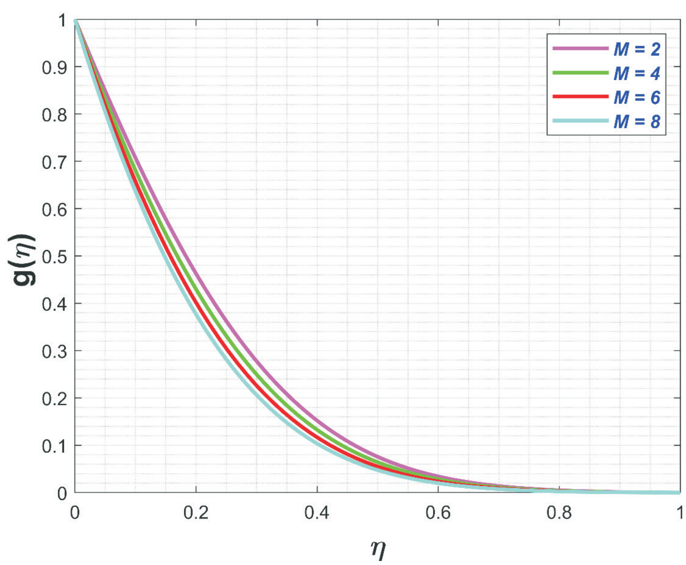

FIGURE 7. The consequence of M on $g(\eta)$.

Figure 8, illustrates the impact of Re on the $h'(\eta)$. The representation indicates that an increase in Re generally results in an elevation of flow velocity, owing to enhanced inertial force effects. However, at a certain threshold, there is a significant reduction in the velocity profile. As Re increases, the influence of viscous forces diminishes, resulting in reduced momentum transfer within the flow field.

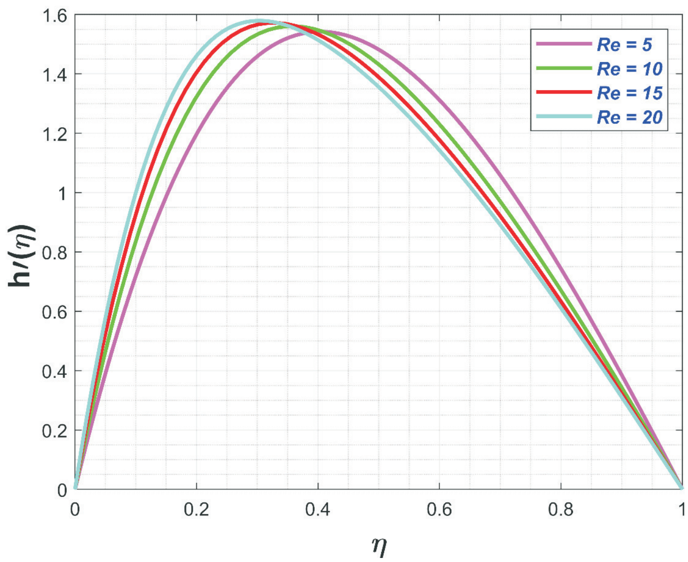

FIGURE 8. The consequence of Re on $h'(\eta)$.

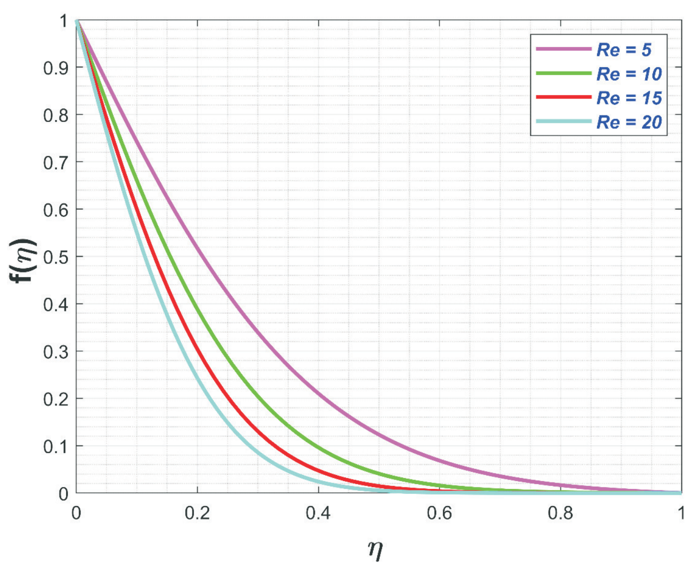

FIGURE 9. The consequence of Re on $f(\eta)$.

Figures 9 and 10 illustrate the fluctuations in the velocity components $f(\eta)$ and $g(\eta)$ as a function of the Re. A rise in the Re corresponds to a significant decrease in the values of both velocity distributions. Higher Re diminish the influence of viscous forces on the system, hence inhibiting momentum transfer between adjacent fluid layers. This results in a diminution of both rotational and axial fluxes.

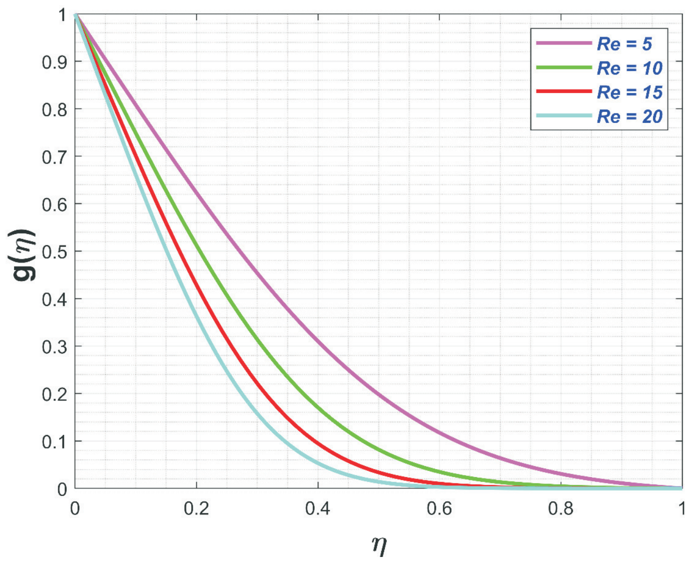

FIGURE 10. The consequence of Re on $g(\eta)$.

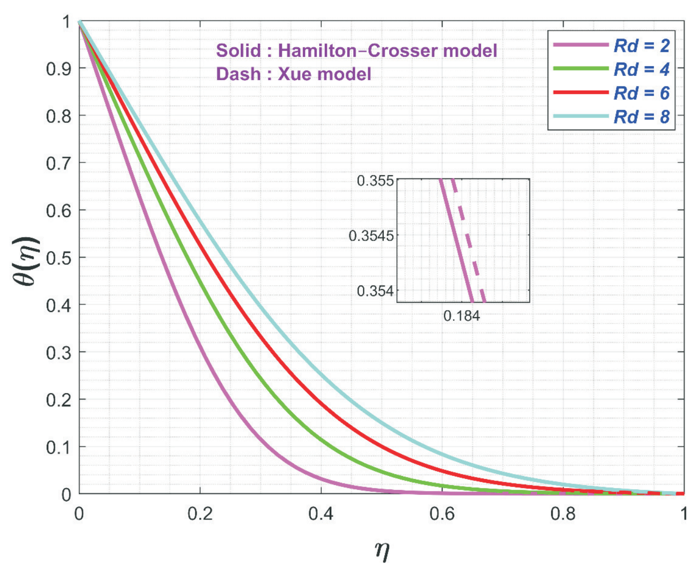

FIGURE 11. The consequence of Rd on $\theta(\eta)$.

Figure 11 illustrates the impact of the Rd on the $\theta(\eta)$. As Rd grows, the temperature profile expands outward to higher values, indicating an overall enhancement in the temperature distribution across the domain. This occurs because increased heat is transferred through radiation in the fluid when the Rd is elevated. Consequently, the thickness of the thermal boundary layer increases with temperature. The Xue model

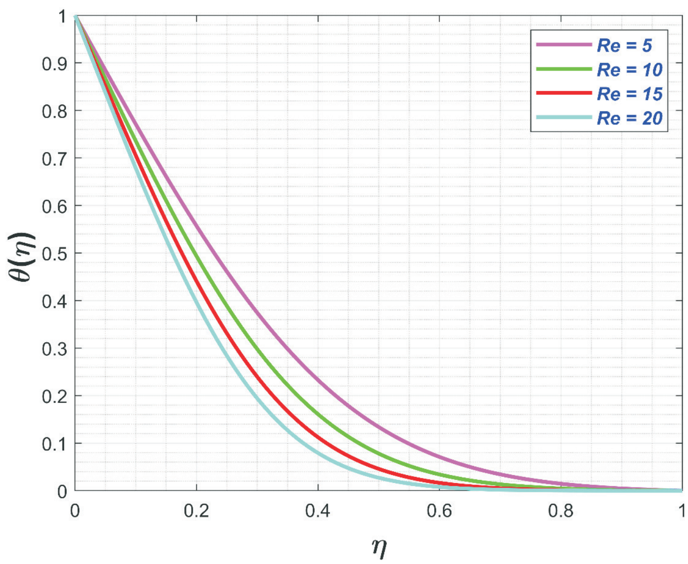

FIGURE 12. The consequence of Re on $\theta(\eta)$.

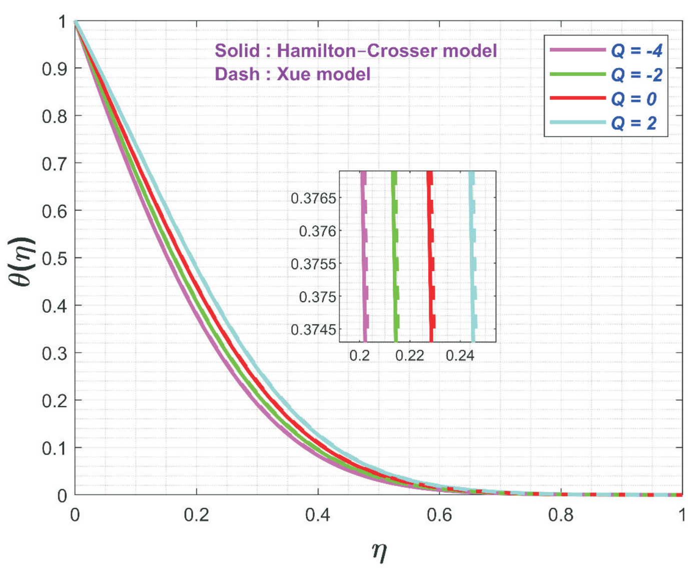

FIGURE 13. The consequence of Q on $\theta(\eta)$.

incorporates anisotropic particle dispersion and interfacial resistance effects, which enhance radiative absorption and energy retention, leading to higher temperatures than the Hamilton Crosser.

Figure 12 illustrates the influence of Re on the $\theta(\eta)$. The results indicate a reduction in fluid temperature as the Re increases. A high Re indicates a greater ratio of inertial to viscous forces in the flow. Consequently, the fluid's viscosity diminishes, leading to a decrease in the heat transmission process.

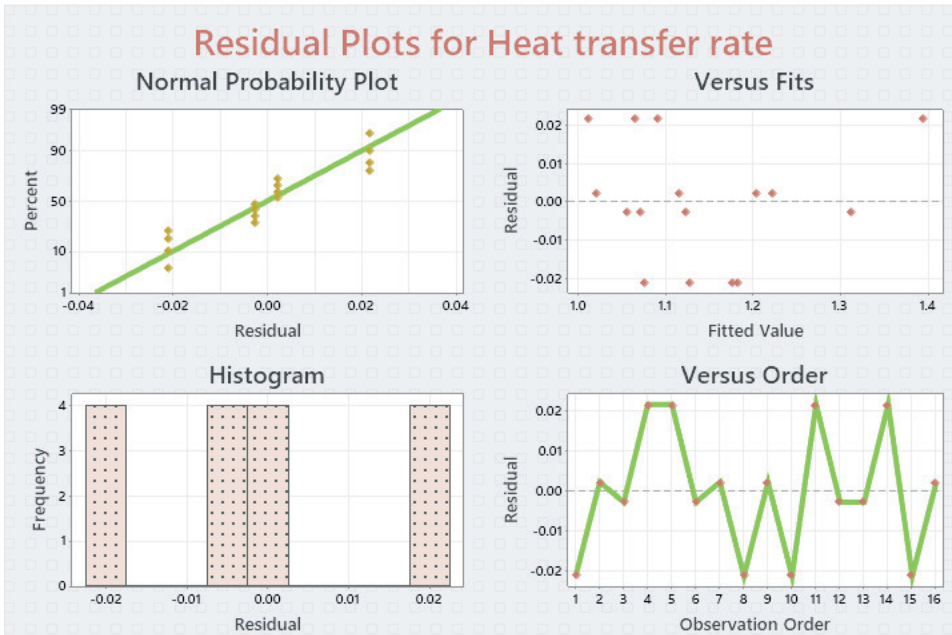

FIGURE 14. Residual plot for $-\theta'(0)$.

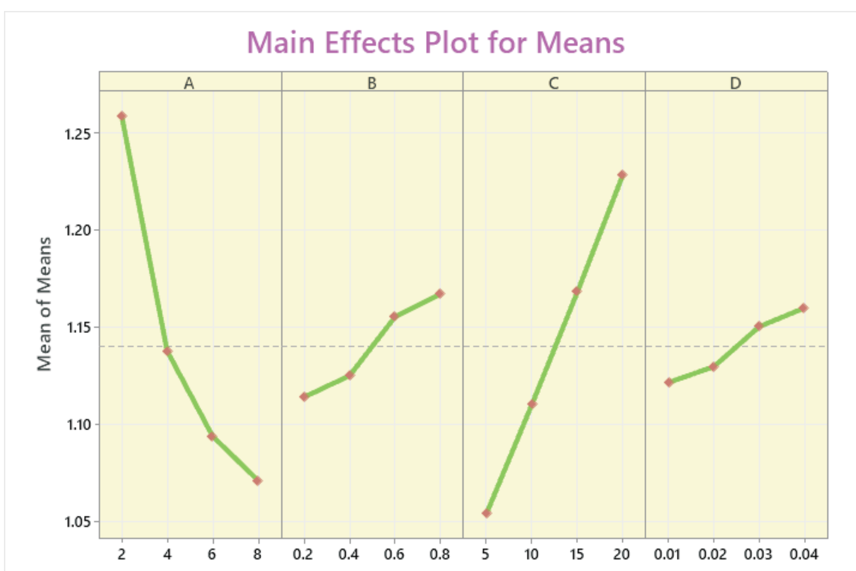

FIGURE 15. Main effect plot of means for governing parameters.

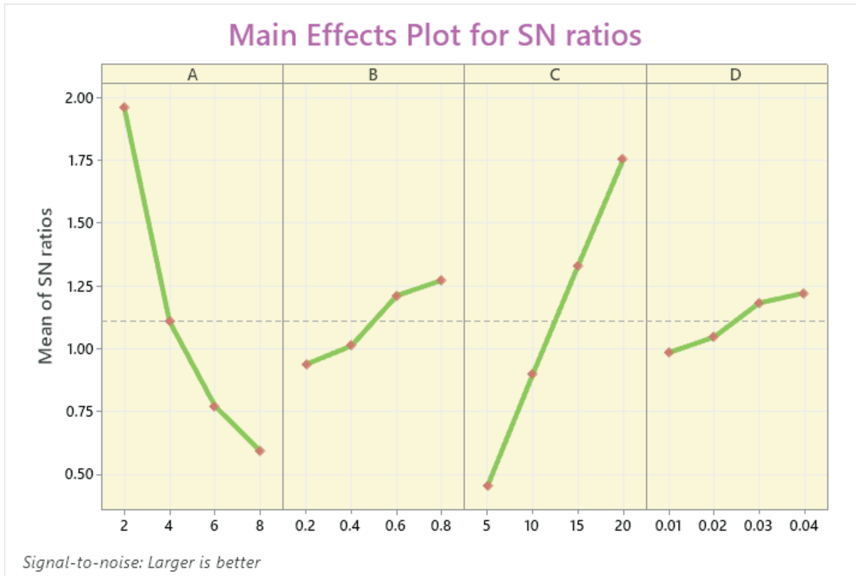

FIGURE 16. Main effect plot of SN ratios for governing parameters.

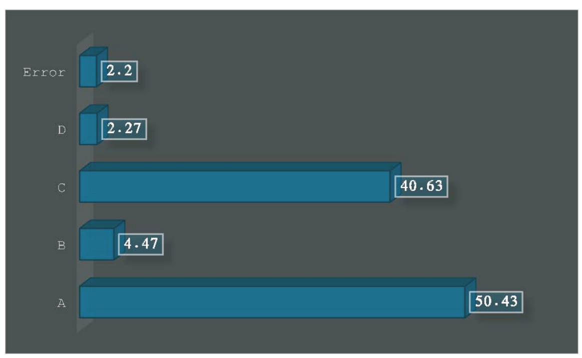

FIGURE 17. Percentage contribution of influential parameters.

As Q increases, Figure 13 demonstrates a significant rise in the $\theta(\eta)$, although heat absorption exhibits an inverse impact. The fluid absorbs additional thermal energy from internal heat generation, resulting in an increased thickness of the thermal barrier layer. Conversely, heat absorption dissipates energy and accelerates cooling. The Xue model incorporates enhanced interfacial hydrogen-thermal and particle interaction effects, increasing internal heat generation and absorption, which leads to more significant temperature variations than the H-C model. The residual plot for $-\theta'(0)$ is visualized in Figure 14. The main effects for mean and SN rations are demonstrated in Figures 15 and 16. The impact of influential parameters on $-\theta'(0)$ is visualized in Figure 17.

6. Conclusion

The primary objective of this study is to investigate the thermal flow characteristics of NF-F over a porous slider with the consideration of radiative effects, magnetic influences and HS-S phenomena. A comparative study has been performed to investigate the effect of T-C caused by Hamilton-Crosser model and Xue model. A suitable similarity transformation has been used to transform the dimensional PDEs to ODEs. The resulting ODEs are solved by the shooting method and RKF-45 method. The Taguchi optimization technique is used to determine the factors influencing H-TR and to ascertain the optimum parameters values. Graphical results are used to analyze the effect of the control parameters on the flow and heat transfer characteristics. The conclusions of the present investigation are the following:

- As the M-F parameter increases, the velocity distribution along the longitudinal direction shows a significant gradient towards the channel centre with a small gradient near the upper and lower surfaces.
- The velocity distributions decrease with increasing wall dilation parameter. Moreover, the injected particles possess an increased probability migrating from the base towards the walls of the slider.
- As the Reynolds number increases, the influence of viscosity to the nanofluid flow becomes less significant and resulting in less molecular energy transfer, and decline in the thermal distribution.
- An increase in the values of the TR parameter indicates a more significant influence of radiative heat transfer on overall heat transfer processes.
- The effectiveness of the statistical technique used to develop the best prediction model for the $-\theta'(0)$, which included many different factors.
- The optimal $-\theta'(0)$ of 1.41595 is achieved by the optimisation method at $Rd = 2$, $Q = 0.8$, $Re = 20$, and $\varphi = 0.04$.
- The radiation parameter accounts for the majority of the H-TR (50.43%), whereas the nanoparticle volume fraction contributes minimally (2.27%).

Acknowledgments

We would like to express our thanks to the Reviewers for their constructive and interesting comments.

References

[1] K. A. M. Alharbi, N. Shaheen, M. Ramzan, S. Kadry, and A. M. Saeed, *Hamilton–Crosser model impact for particle shape in a nanofluid flow influenced by variable thermal conductivity*, Numerical Heat Transfer, Part B: Fundamentals, **87**(1) (2026), 601–619.

[2] B. S. T. Alkahtani, R. J. Punith Gowda, S. S. Alzaid, N. Sharma, and J. Madhu, *Impact of chemical reactions that generate and absorb heat in the flow induced by a squeezing porous slider*, Physica Scripta, **99**(7) (2024), Article Id: 075247.

[3] M. S. Anwar, T. Muhammad, M. Khan, and V. Puneeth, *MHD nanofluid flow through Darcy medium with thermal radiation and heat source*, International Journal of Modern Physics B, **38** (2024), Article Id: 2450386.

[4] M. I. Asjad, M. Zahid, M. Inc, D. Baleanu, and B. Almohsen, *Impact of activation energy and MHD on Williamson fluid flow in the presence of bioconvection*, Alexandria Engineering Journal, **61**(11) (2022), 8715–8727.

[5] R. C. Bataller, *Viscoelastic fluid flow and heat transfer over a stretching sheet under the effects of a non-uniform heat source, viscous dissipation and thermal radiation*, International Journal of Heat and Mass Transfer **50**(15–16), (2007), 3152–3162.

[6] M. Bharath Kumar, M. Vijaya Kumar, M. Nagapavani, M. Varuna and P. Siva Kota Reddy, *Artificial neural network and Sigmoid polynomial-based method for chemically reactive fluid flow mechanism between upper stationary and lower rotating disk*, International Journal of Thermofluids, 34 (2026), Article Id: 101646, 18 Pages.

[7] A. M. Darbari and M. A. Alavi, *Application of Taguchi method in the numerical analysis of fluid flow and heat transfer around a flat tube with various axial ratios*, International Communications in Heat and Mass Transfer, **126** (2021), Article Id: 105472.

[8] Y. Dharmendar Reddy, B. Shankar Goud, K. S. Nisar, B. Alshahrani, M. Mahmoud, and C. Park, *Heat absorption/generation effect on MHD heat transfer fluid flow along a stretching cylinder with a porous medium*, Alexandria Engineering Journal, **64** (2023), 659–666.

[9] A. M. Galal, A. Mabrouk, H. F. M. Ameen, M. Abbas, D. L. C. Ching, M. S. Sajjad, A. A. Faqihi, L. Kolsi, A. A. Memon and I. Khan, *Optimizing flow and heat transfer in industrial processes: The potential of trihybrid nanofluid and thermal-radiation using Hamilton-Crosser and Xue models*, Journal of Radiation Research and Applied Sciences, **18**(1) (2025), Article Id: 101322.

[10] N. Faraz, Y. Khan, A. Anjum, and M. Kahshan, *Three-Dimensional Hydro-Magnetic Flow Arising in a Long Porous Slider and a Circular Porous Slider with Velocity Slip*, Mathematics, **7**(8) (2019), Article Number: 748, 23 Pages.

[11] N. Faraz, Y. Khan, and A. Anjum, *A statistical and numerical analysis of porous sliders modeling under a transverse magnetic field with slip conditions*, Multidiscipline Modeling in Materials and Structures, **21**(5) (2025), 1170–1194.

[12] M. Izadi, N. M. Maleki, I. Pop, and S. A. M. Mehryan, *Natural convection of a hybrid nanofluid subjected to non-uniform magnetic field within porous medium including circular heater*, International Journal of Numerical Methods for Heat & Fluid Flow **29**(4) (2019), 1211–1231.

[13] M. A. Kumar, Y. D. Reddy, V. S. Rao, and B. S. Goud, *Thermal radiation impact on MHD heat transfer natural convective nano fluid flow over an impulsively started vertical plate*, Case Studies in Thermal Engineering, **24** (2021), Article Id: 100826, 10 Pages.

[14] P. Kumar, B. Nagaraja, A. R. Ajaykumar and F. Almeida, *Optimization design based on Taguchi method and statistical analysis of variance for thermo-diffusive flow over a curved sheet: entropy analysis*, International Journal of Modelling and Simulation, 0(0) (2024), Article Id: 2437829, 20 Pages.

[15] M. Madani, Y. Khan, Gh. Mahmodi, N. Faraz, A. Yildirim, and B. Nasernejad, Application of homotopy perturbation and numerical methods to the circular porous slider, Int. J. Numer. Methods Heat Fluid Flow, **22**(6) (2012), 705–717.

[16] M. A. A. Mahmoud, *Thermal radiation effects on MHD flow of a micropolar fluid over a stretching surface with variable thermal conductivity*, Physica A: Statistical Mechanics and its Applications, **375**(2) (2007), 401–410.

[17] S. Majumder, T. Chakraborty, and P. K. Kundu, *Taguchi analysis on heat transfer of triple diffusive flow of a nanofluid over a rotating sphere in presence of Hall current*, Proceedings of the Institution of Mechanical Engineers, Part N: Journal of Nanomaterials, Nanoengineering and Nanosystems, (2026), DOI: 10.1177/23977914261426171.

[18] M. K. Mishra, A. Pandey, and S. M. Hussain, *Investigating thermal performance of Marangoni convective nanofluid flow on an infinite porous disk: Numerical and Taguchi optimization techniques*, Proceedings of the Institution of Mechanical Engineers, Part N: Journal of Nanomaterials, Nanoengineering and Nanosystems, (2026), DOI: 10.1177/23977914261426241.

[19] M. Nabhani and M. El Khlifi, *Non-Newtonian inertial magnetohydrodynamic porous squeeze film lubrication between circular discs*, Tribology International, **94** (2016), 373–382.

[20] B. Raei, *Statistical Analysis of Nanofluid Heat Transfer in a Heat Exchanger using Taguchi Method*, Journal of Heat and Mass Transfer Research, **8**(1) (2021), 29–38.

[21] N. Sandeep, S. Lingamurthy and K. Anantha Kumar, *Optimal usage of solar energy in cylindrical film flow of Prandtl ferrofluid: a relative analysis of Hamilton-Crosser and Xue nano models*, Multidiscipline Modeling in Materials and Structures, **22**(3), (2025), 610–626.

[22] M. Sarfraz, M. Yasir, and M. Khan, *Exploring dual solutions and thermal conductivity in hybrid nanofluids: a comparative study of Xue and Hamilton–Crosser models*, Nanoscale Advances, **5** (2023), 6695–6704.

[23] T. Sravan Kumar, D. N. Punith Kumar and A. Sreevallabha Reddy, *Study of mixed convective–radiative fluid flow in a channel with temperature-dependent thermal conductivity*, Partial Differential Equations in Applied Mathematics, **5** (2022), Article Id: 100344, 7 Pages.

[24] G. K. Tejaswini, K. Vinutha, J. K. Madhukesh, P. Siva Kota Reddy and Umair Khan, *RKF45 optimization for the boundary layer hybrid nanofluid flows of stationary and moving flat plates with chemical reactions*, Discover Applied Sciences, **8** (2026), Article Number: 334, 18 Pages.

[25] M. Turkyilmazoglu, *Three dimensional viscous flow due to a squeezing porous slider*, European Journal of Mechanics-B/Fluids, **98** (2023), 253–259.

[26] Z. Ullah, M. Ehsan, H. Ahmad, and A. Ilyas, *Combined effects of MHD and slip velocity on oscillatory mixed convective flow around a non-conducting circular cylinder embedded in a porous medium*, Case Studies in Thermal Engineering, **38** (2022), Article Id: 102341.

[27] H. Wang, Z. Rao, W. Wang, and S. Liao, *A reconstruction of Hamilton-Crosser model for effective thermal conductivity of nanofluids based on particle clustering and nanolayer formation*, Case Studies in Thermal Engineering, **26** (2021), Article Id: 101051.

G. J. Manjula, Department of Mathematics, Siddaganga Institute of Technology, Tumukuru-572 103, Karnataka, India.
Email address: gjm@sit.ac.in

M. Kirankumar, Department of Mathematics, Vidyavardhaka College of Engineering, Mysuru-570 006, Karnataka, India.
Email address: kiran.maths@vvce.ac.in

M. J. Sridevi, Department of Mathematics, Government First Grade College for Women, Hassan-573 201, Karnataka, India.
Email address: thanusri.j@gmail.com

R. D. Jagadeesha, Department of Mathematics, Government First Grade College for Women, Holenarasipura-573 211, Karnataka, India.
Email address: jagdeesh25@gmail.com

Radhika M., Department of Mathematics, Government First Grade College, Kolar Gold Fields-563 122, Karnataka, India.
Email address: radhika.manghat@gmail.com

C. G. Jagannatha, Department of Mathematics, HPPC Government First Grade College, Challakere-577 501, Karnataka, India.
Email address: cgjagannath@gmail.com

K. C. Jagadeesha, Department of Mathematics, Government First Grade College, Tumkur-572 102, Karnataka, India.
Email address: kcjagadish.09@gmail.com

Rekha J., Department of Mathematics, Cambridge Institute of Technology, Bengaluru-560 036, Karnataka, India.
Email address: rekha.maths@cambridge.edu.in